Search for Spectral Irregularities due to Photon–Axionlike-Particle Oscillations with the Fermi Large Area Telescope

M. Ajello,[1] A. Albert,[2] B. Anderson,[3,4] L. Baldini,[5,2] G. Barbiellini,[6,7] D. Bastieri,[8,9] R. Bellazzini,[10] E. Bissaldi,[11] R. D. Blandford,[2] E. D. Bloom,[2] R. Bonino,[12,13] E. Bottacini,[2] J. Bregeon,[14] P. Bruel,[15] R. Buehler,[16] G. A. Caliandro,[2,17] R. A. Cameron,[2] M. Caragiulo,[18,11] P. A. Caraveo,[19] C. Cecchi,[20,21] A. Chekhtman,[22,§] S. Ciprini,[23,20] J. Cohen-Tanugi,[14] J. Conrad,[3,4,*] F. Costanza,[11] F. D'Ammando,[24,25] A. de Angelis,[26] F. de Palma,[11,27] R. Desiante,[28,12] M. Di Mauro,[2] L. Di Venere,[18,11] A. Domínguez,[1] P. S. Drell,[2] C. Favuzzi,[18,11] W. B. Focke,[2] A. Franckowiak,[2] Y. Fukazawa,[29] S. Funk,[30] P. Fusco,[18,11] F. Gargano,[11] D. Gasparrini,[23,20] N. Giglietto,[18,11] T. Glanzman,[2] G. Godfrey,[2] S. Guiriec,[31] D. Horan,[15] G. Jóhannesson,[32] M. Katsuragawa,[33] S. Kensei,[29] M. Kuss,[10] S. Larsson,[34,4] L. Latronico,[12] J. Li,[35] L. Li,[34,4] F. Longo,[6,7] F. Loparco,[18,11] P. Lubrano,[20] G. M. Madejski,[2] S. Maldera,[12] A. Manfreda,[10] M. Mayer,[16] M. N. Mazziotta,[11] M. Meyer,[3,4,†] P. F. Michelson,[2] N. Mirabal,[31] T. Mizuno,[36] M. E. Monzani,[2] A. Morselli,[37] I. V. Moskalenko,[2] S. Murgia,[38] M. Negro,[12,13] E. Nuss,[14] C. Okada,[29] E. Orlando,[2] J. F. Ormes,[39] D. Paneque,[40,2] J. S. Perkins,[31] M. Pesce-Rollins,[10,2] F. Piron,[14] G. Pivato,[10] T. A. Porter,[2] S. Rainò,[18,11] R. Rando,[8,9] M. Razzano,[10] A. Reimer,[41,2] M. Sánchez-Conde,[4,3,‡] C. Sgrò,[10] D. Simone,[11] E. J. Siskind,[42] F. Spada,[10] G. Spandre,[10] P. Spinelli,[18,11] H. Takahashi,[29] J. B. Thayer,[2] D. F. Torres,[35,43] G. Tosti,[20,21] E. Troja,[31,44] Y. Uchiyama,[45] K. S. Wood,[46] M. Wood,[2] G. Zaharijas,[47,48] and S. Zimmer[3,4]

(The Fermi-LAT Collaboration)

[1]*Department of Physics and Astronomy, Clemson University, Kinard Lab of Physics, Clemson, South Carolina 29634-0978, USA*
[2]*W. W. Hansen Experimental Physics Laboratory, Kavli Institute for Particle Astrophysics and Cosmology, Department of Physics and SLAC National Accelerator Laboratory, Stanford University, Stanford, California 94305, USA*
[3]*Department of Physics, Stockholm University, AlbaNova, SE-106 91 Stockholm, Sweden*
[4]*The Oskar Klein Centre for Cosmoparticle Physics, AlbaNova, SE-106 91 Stockholm, Sweden*
[5]*Università di Pisa and Istituto Nazionale di Fisica Nucleare, Sezione di Pisa I-56127 Pisa, Italy*
[6]*Istituto Nazionale di Fisica Nucleare, Sezione di Trieste, I-34127 Trieste, Italy*
[7]*Dipartimento di Fisica, Università di Trieste, I-34127 Trieste, Italy*
[8]*Istituto Nazionale di Fisica Nucleare, Sezione di Padova, I-35131 Padova, Italy*
[9]*Dipartimento di Fisica e Astronomia "G. Galilei," Università di Padova, I-35131 Padova, Italy*
[10]*Istituto Nazionale di Fisica Nucleare, Sezione di Pisa, I-56127 Pisa, Italy*
[11]*Istituto Nazionale di Fisica Nucleare, Sezione di Bari, I-70126 Bari, Italy*
[12]*Istituto Nazionale di Fisica Nucleare, Sezione di Torino, I-10125 Torino, Italy*
[13]*Dipartimento di Fisica Generale "Amadeo Avogadro," Università degli Studi di Torino, I-10125 Torino, Italy*
[14]*Laboratoire Univers et Particules de Montpellier, Université Montpellier, CNRS/IN2P3, Montpellier, France*
[15]*Laboratoire Leprince-Ringuet, École polytechnique, CNRS/IN2P3, Palaiseau, France*
[16]*Deutsches Elektronen Synchrotron DESY, D-15738 Zeuthen, Germany*
[17]*Consorzio Interuniversitario per la Fisica Spaziale (CIFS), I-10133 Torino, Italy*
[18]*Dipartimento di Fisica "M. Merlin" dell'Università e del Politecnico di Bari, I-70126 Bari, Italy*
[19]*INAF-Istituto di Astrofisica Spaziale e Fisica Cosmica, I-20133 Milano, Italy*
[20]*Istituto Nazionale di Fisica Nucleare, Sezione di Perugia, I-06123 Perugia, Italy*
[21]*Dipartimento di Fisica, Università degli Studi di Perugia, I-06123 Perugia, Italy*
[22]*College of Science, George Mason University, Fairfax, Virginia 22030, USA and Naval Research Laboratory, Washington, D.C. 20375, USA*
[23]*Agenzia Spaziale Italiana (ASI) Science Data Center, I-00133 Roma, Italy*
[24]*INAF Istituto di Radioastronomia, I-40129 Bologna, Italy*
[25]*Dipartimento di Astronomia, Università di Bologna, I-40127 Bologna, Italy*
[26]*Dipartimento di Fisica, Università di Udine and Istituto Nazionale di Fisica Nucleare, Sezione di Trieste, Gruppo Collegato di Udine, I-33100 Udine*
[27]*Università Telematica Pegaso, Piazza Trieste e Trento, 48, I-80132 Napoli, Italy*
[28]*Università di Udine, I-33100 Udine, Italy*
[29]*Department of Physical Sciences, Hiroshima University, Higashi-Hiroshima, Hiroshima 739-8526, Japan*
[30]*Erlangen Centre for Astroparticle Physics, D-91058 Erlangen, Germany*
[31]*NASA Goddard Space Flight Center, Greenbelt, Maryland 20771, USA*
[32]*Science Institute, University of Iceland, IS-107 Reykjavik, Iceland*
[33]*Institute of Space and Astronautical Science, Japan Aerospace Exploration Agency, 3-1-1 Yoshinodai, Chuo-ku, Sagamihara, Kanagawa 252-5210, Japan*

[34]Department of Physics, KTH Royal Institute of Technology, AlbaNova, SE-106 91 Stockholm, Sweden
[35]Institute of Space Sciences (IEEC-CSIC), Campus UAB, E-08193 Barcelona, Spain
[36]Hiroshima Astrophysical Science Center, Hiroshima University, Higashi-Hiroshima, Hiroshima 739-8526, Japan
[37]Istituto Nazionale di Fisica Nucleare, Sezione di Roma "Tor Vergata," I-00133 Roma, Italy
[38]Center for Cosmology, Physics and Astronomy Department, University of California, Irvine, California 92697-2575, USA
[39]Department of Physics and Astronomy, University of Denver, Denver, Colorado 80208, USA
[40]Max-Planck-Institut für Physik, D-80805 München, Germany
[41]Institut für Astro- und Teilchenphysik and Institut für Theoretische Physik, Leopold-Franzens-Universität Innsbruck, A-6020 Innsbruck, Austria
[42]NYCB Real-Time Computing Inc., Lattingtown, New York 11560-1025, USA
[43]Institució Catalana de Recerca i Estudis Avançats (ICREA), Barcelona, Spain
[44]Department of Physics and Department of Astronomy, University of Maryland, College Park, Maryland 20742, USA
[45]Department of Physics, 3-34-1 Nishi-Ikebukuro, Toshima-ku, Tokyo 171-8501, Japan
[46]Space Science Division, Naval Research Laboratory, Washington, D.C. 20375-5352, USA
[47]Istituto Nazionale di Fisica Nucleare, Sezione di Trieste, and Università di Trieste, I-34127 Trieste, Italy
[48]Laboratory for Astroparticle Physics, University of Nova Gorica, Vipavska 13, SI-5000 Nova Gorica, Slovenia
(Received 27 November 2015; published 20 April 2016)

We report on the search for spectral irregularities induced by oscillations between photons and axionlike-particles (ALPs) in the γ-ray spectrum of NGC 1275, the central galaxy of the Perseus cluster. Using 6 years of Fermi Large Area Telescope data, we find no evidence for ALPs and exclude couplings above 5×10^{-12} GeV^{-1} for ALP masses $0.5 \lesssim m_a \lesssim 5$ neV at 95% confidence. The limits are competitive with the sensitivity of planned laboratory experiments, and, together with other bounds, strongly constrain the possibility that ALPs can reduce the γ-ray opacity of the Universe.

DOI: 10.1103/PhysRevLett.116.161101

Introduction.—Axions and axionlike-particles (ALPs) are predicted by a variety of extensions of the standard model [1–6]. If produced nonthermally in the early Universe, these particles may account for all or a significant fraction of the cold dark matter (DM) (see, e.g., Refs. [7–10]), and could be detected through their coupling to photons in magnetic fields [11,12]. While the axion mass is proportional to its coupling to photons, these two parameters are independent in the case of ALPs.

Photon-ALP interactions could leave an imprint on γ-ray spectra, provided that the ALP mass is sufficiently small, $m_a \lesssim \mu$eV. Above a critical energy $E_{\rm crit}$, photon-ALP mixing becomes maximal, leading to a reduction of the photon flux [13–15]. Around $E_{\rm crit}$ this is accompanied by spectral irregularities that depend on the strength and morphology of the magnetic field [16]. Photon-ALP conversions could also reduce the opacity of the Universe caused by pair production of γ rays with photons of the extragalactic background light (EBL) [17,18]. Evidence exists that the γ-ray absorption is indeed lower than expected from state-of-the-art EBL models [19–22], and ALPs have been used to explain these observations [17,18,23–26] (see, however, Refs. [27,28]).

Sources embedded in galaxy clusters are promising to search for ALPs due to the strong magnetic fields extending over large spatial scales in these systems. For example, the absence of irregularities above 200 GeV in the spectrum of the blazar PKS 2155-304, associated with a poor galaxy cluster, has been used to constrain the photon-ALP coupling [29]. Here, we focus on the search for irregularities in the spectrum of the radio galaxy NGC 1275 with the Fermi Large Area Telescope (LAT). NGC 1275 is the most favorable target since it is a bright γ-ray emitter detected with a significance exceeding 100σ in the third Fermi-LAT source catalog (3FGL) [30]. Its broadband emission can be explained with synchrotron self-Compton models, which predict a smooth γ-ray spectrum [31,32]. It is located at the center of the Perseus cool-core cluster for which rotation measures (RMs) suggest a high central magnetic field [33].

Our analysis makes use of the newest PASS 8 event-level analysis for LAT data. Compared to previous passes, PASS 8 has an improved angular resolution, a broader energy range, larger effective area, as well as reduced uncertainties in the instrumental response functions (IRFs) [34].

LAT data selection.—We make use of 6 years of LAT data taken between Aug. 4, 2008 and Aug. 4, 2014 in the energy range from 100 MeV to 500 GeV. For lower energies, the effective area decreases rapidly and the energy dispersion increases. At energies above 500 GeV we do not expect sufficient photon statistics [35]. We only consider events that arrive at a zenith angle $\theta_z < 90°$ in order to minimize the contribution of γ rays from the Earth limb. Time intervals that correspond to bright solar flares and γ-ray bursts are excluded. We extract γ-ray-like events within a $10° \times 10°$ region of interest (ROI) centered at the position of NGC 1275: $\alpha_{2000} = 3^{\rm h}19^{\rm m}49.9^{\rm s}$, $\delta_{2000} = +41°30'49.2''$ [30].

Events passing the PASS 8 P8R2_SOURCE selection cuts are analyzed using the P8R2_SOURCE_V6 IRFs [36]. An innovation of the PASS 8 IRFs is the possibility to subdivide an event class into event types according to the quality of the angular or energy reconstruction [point spread function (PSF) and energy dispersion (EDISP) event types, respectively]. In this analysis we will use the EDISP types to maximize our sensitivity to spectral irregularities. Events are classified into one of four types ranging from EDISP0 to EDISP3 that denote the quality of the energy reconstruction from worst to best. All EDISP event types have a similar number of events in each logarithmic energy bin and are mutually exclusive. The energy dispersion matrices are given in the Supplemental Material [37].

Photon-ALP oscillations.—Following Refs. [20,49–52], we derive the probability $P_{\gamma\gamma}$ for a final state photon in the photon-ALP beam as a function of energy for an initially unpolarized photon beam (see the Supplemental Material [37]). We expect the irregularities to occur around a critical energy [15],

$$E_{\rm crit} \sim 2.5\ {\rm GeV}\frac{|m^2_{a,{\rm neV}} - \omega^2_{\rm pl,neV}|}{g_{11}B_{\mu{\rm G}}}, \qquad (1)$$

with ALP mass $m_{a,{\rm neV}}$ and plasma frequency $\omega_{\rm pl,neV}$ in units of neV, coupling constant $g_{11} = g_{a\gamma}/10^{-11}\ {\rm GeV}^{-1}$, and magnetic field $B_{\mu{\rm G}} = B/1\mu{\rm G}$. We include photon-ALP mixing in the intracluster and galactic magnetic fields [17,42]. The B field of the Milky Way is modeled with the coherent component of the model described in Ref. [53]. We do not include its turbulent component, as the scales on which the turbulence occurs are usually smaller than the photon-ALP oscillation length. The turbulent intracluster B field is described below. Absorption of γ rays by the EBL is taken into account through the model of Ref. [54]. We neglect any oscillations in the intergalactic magnetic field (IGMF). With current upper limits on the IGMF strength of $\lesssim 10^{-9}$ G and on the photon-ALP coupling, $g_{11} < 6.6$ [55], we find that $E_{\rm crit} \lesssim 100$ GeV only for $m_{a,{\rm neV}} \lesssim 0.5$. For such low masses, g_{11} is further constrained below 0.6 from the nonobservation of γ rays from SN 1987A [56]. Given this small coupling and the comparatively short distance to NGC 1275 (redshift $z = 0.017559$), no strong irregularities should be induced by mixing in the IGMF.

Intracluster magnetic field.—Faraday RM observations and magnetohydrodynamic simulations suggest that the magnetic field in galaxy clusters is turbulent and that its strength follows the electron density $n_e(r)$ of the intracluster medium, $B(r) = B_0[n_e(r)/n_e(r=0)]^\eta$ [57–59]. We model the turbulent component as a divergence-free homogeneous isotropic field with Gaussian turbulence with zero mean and a variance σ_B [52]. The energy density follows a power law $M(k) \propto k^q$ in wave numbers k. It is nonzero only between the minimum and maximum turbulence scales $k_L = 2\pi/\Lambda_{\rm max}$ and $k_H = 2\pi/\Lambda_{\rm min}$.

For the Perseus cluster, we use $n_e(r)$ derived from x-ray observations [Eq. (4) in Ref. [60]] within the inner $r_{\rm max} = 500$ kpc. Beyond this radius, we conservatively assume a zero magnetic field. RMs currently only probe the innermost region (tens of pc) around NGC 1275. The observations lead to an estimated central magnetic field of 25 μG [33]. An independent lower limit of $B_0 \gtrsim 2$–13 μG for $0.3 \le \eta \le 0.7$ has been derived from MAGIC Collaboration observations of the Perseus cluster [61]. These results motivate our assumptions for $\sigma_B = 10\ \mu$G and $\eta = 0.5$, which are also in line with observations of other cool-core clusters (see, e.g., Refs. [62,63]).

For the turbulence spectrum, we assume values derived from RMs of the cool-core cluster A2199 [63], which has a comparable number of member galaxies. The fiducial parameter choices are summarized in Table I.

Data analysis.—We perform a binned Poisson likelihood analysis, similar to the DM signal search from dwarf spheroidal galaxies [64,65]. Events are binned into $10^\circ \times 10^\circ$ sky maps with a resolution of 0.2° per pixel. The width of the logarithmically spaced energy bins is chosen to be 30% of the median energy resolution of each EDISP event type (see the Supplemental Material for details [37]). This results in 39, 67, 94, and 145 energy bins for EDISP0–3, respectively. We have tested with simulations that bin sizes below 40% of the median energy resolution do not affect the results.

For each event type, we perform a fit over the entire energy range and ROI for all source parameters (nuisance parameters $\boldsymbol{\theta}_i$) using *gtlike* included in the Fermi-LAT SCIENCE TOOLS version v10r01p01 [66]. We include all point sources listed in the 3FGL within 15° from the ROI center. The diffuse backgrounds are modeled with templates for the galactic and the isotropic extragalactic γ-ray emission [67]. The energy dispersion is taken into account in the fitting of the point sources whereas it is already accounted for in the data-driven derivation of the diffuse templates. Normalizations of the diffuse sources and point sources within 8° from the ROI center are left free to vary. All spectral indices of the point sources within 4° are also free parameters. The time-averaged spectrum of NGC 1275

TABLE I. Fiducial model parameters for the intracluster magnetic field in Perseus.

Parameter	Value
σ_B	10 μG
$r_{\rm max}$	500 kpc
η	0.5
q	−2.8
$\Lambda_{\rm min}$	0.7 kpc
$\Lambda_{\rm max}$	35 kpc

is modeled with a logarithmic (log) parabola, $F(E) = N(E/E_0)^{-[\alpha+\beta\ln(E/E_0)]}$, where E_0 is fixed to 530 MeV [30].

Under the assumption that the profiled nuisance parameters do not change when considering each bin separately [64], we extract the likelihood in each reconstructed energy bin k', $\mathcal{L}(\mu_{ik'}, \boldsymbol{\theta}_i | D_{ik'})$ as a function of expected counts $\mu_{ik'}$ of NGC 1275, and observed counts $D_{ik'}$. For NGC 1275 a power law with fixed spectral index $\Gamma = 2$ is now assumed in each bin. For each tested value of $\mu_{ik'}$ we reoptimize the normalization of the spectrum of the radio galaxy IC 310, which has an angular separation of ~0.6° from NGC 1275.

Under the ALP hypothesis, characterized by $P_{\gamma\gamma} \equiv P_{\gamma\gamma}(E, m_a, g_{a\gamma}, \mathbf{B}_j)$ for one random turbulent B-field realization $\mathbf{B}_j$, the expected number of photons is calculated through

$$\mu_{ik'} = \sum_k \mathcal{D}^i_{kk'} \int_{\Delta E_k} dE P_{\gamma\gamma} F(E) \mathcal{E}^i(E), \tag{2}$$

where the integration runs over the true energy bin ΔE_k, $\mathcal{E}^i$ is the exposure, and $\mathcal{D}^i_{kk'}$ is the energy dispersion for event type EDISPi. Under the null hypothesis, $P_{\gamma\gamma}$ reduces to the EBL attenuation. The parameters of the intrinsic source spectrum $F(E)$, N, α, and β, are further nuisance parameters. For each tested ALP parameter and magnetic field, we determine these parameters by profiling the joint likelihood of all energy bins k',

$$\mathcal{L}_i(\boldsymbol{\mu}, \boldsymbol{\theta} | \mathbf{D}) \equiv \prod_{k'} \mathcal{L}(\mu_{ik'}, \boldsymbol{\theta}_i | D_{ik'}), \tag{3}$$

for each event type separately, using the precomputed likelihood curves $\mathcal{L}(\mu_{ik'}, \boldsymbol{\theta}_i | D_{ik'})$. In this way, we treat each event type selection as an independent measurement [68]. The bin-by-bin likelihood curves for the EDISP3 event type are shown in Fig. 1 together with the best-fit spectra.

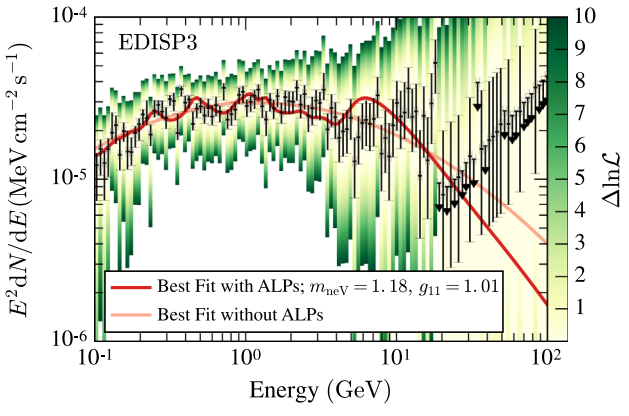

FIG. 1. The likelihood curves (shown in color) for the EDISP3 event type. $\Delta \ln \mathcal{L} = 0$ corresponds to the maximum likelihood in each bin (black points). The error bars indicate an increase of the likelihood by $2\Delta \ln \mathcal{L} = 1$. The best-fit spectrum of the joint likelihood without an ALP (with an ALP with $m_{\rm neV} = 1.2$ and $g_{11} = 1$) is shown as a light (dark) red solid line.

We simulate $N_B = 500$ random realizations of the turbulent field $\mathbf{B}_j$, $j = 1, \ldots, N_B$. The dependence of the likelihood on the realizations is not easily parametrizable and we cannot assume that the simulations map the space of possible realizations. Therefore, instead of profiling, we sort the B-field realizations for each tested $(m_a, g_{a\gamma})$ pair by increasing values of the product over the likelihoods $\mathcal{L}_i$ and use the realization that corresponds to the $Q_B = 0.95$ quantile of the likelihood distribution (profiling would correspond to $Q_B = 1$). We will denote this realization as $\mathbf{B}_{95}$ and the corresponding expected counts with $\boldsymbol{\mu}_{95}$. Note that $\mathbf{B}_{95}$ might be different for different ALP parameters, so that $\mathbf{B}_{95} \equiv \mathbf{B}_{95}(m_a, g_{a\gamma})$.

Similar to Ref. [69], we evaluate the ALP hypothesis with a likelihood ratio test. The test statistic (TS) for the ALP hypothesis is calculated from the joint likelihood of all event types:

$$\mathrm{TS} = -2 \sum_i \ln \left(\frac{\mathcal{L}_i(\boldsymbol{\mu}_0, \hat{\hat{\boldsymbol{\theta}}} | \mathbf{D})}{\mathcal{L}_i(\hat{\boldsymbol{\mu}}_{95}, \hat{\boldsymbol{\theta}} | \mathbf{D})} \right), \tag{4}$$

where $\boldsymbol{\mu}_0$ are the expected counts for the null (no ALP) hypothesis with maximized nuisance parameters $\hat{\hat{\boldsymbol{\theta}}} \equiv \hat{\boldsymbol{\theta}}(\boldsymbol{\mu}_0)$ and $\hat{\boldsymbol{\mu}}_{95}$ are the expected counts under the ALP hypothesis that, together with $\hat{\boldsymbol{\theta}}$, maximize the likelihoods of each event type. We test ALP parameters on a logarithmic $(m_a, g_{a\gamma})$ grid with (19×12) steps where $0.07 \leq m_{a,\rm neV} \leq 100$ and $0.1 \leq g_{11} \leq 7$. The mass range is chosen such that $E_{\rm crit}$ falls into the analyzed energy range whereas the maximum coupling is motivated by the bound found in Ref. [55]. For the lower bound, the amplitude of the irregularities is too small to be detectable.

In order to convert the TS value into a significance, we need to know the underlying probability distribution. We derive the null distribution from Monte Carlo simulations and from it the threshold TS value, $\mathrm{TS}_{\rm thr}$, for which we can reject the null hypothesis (see the Supplemental Material for details [37]). For a rejection of the no-ALP hypothesis at a 3σ (global) significance level, we find that $\mathrm{TS} > \mathrm{TS}_{\rm thr} = 33.1$.

Results.—The best-fit ALP parameters are found at $m_{\rm neV} = 44.6$ and $g_{11} = 4.76$ with $\mathrm{TS} = 10.40 < \mathrm{TS}_{\rm thr}$, and hence the best fit with ALPs is not significantly preferred over the null hypothesis. We set upper limits by stepping over the ALP parameters and calculating the difference $\lambda(m_a, g_{a\gamma})$ between the log-likelihood values for each pair m_a, $g_{a\gamma}$ and the best fit. ALP parameters are excluded with 95% confidence if $\lambda > \lambda_{\rm thr} = 22.8$. The threshold value $\lambda_{\rm thr}$ is calculated under the assumption that the probability distribution of the alternative hypothesis follows the null distribution. We have tested this assumption with simulations and found that this choice

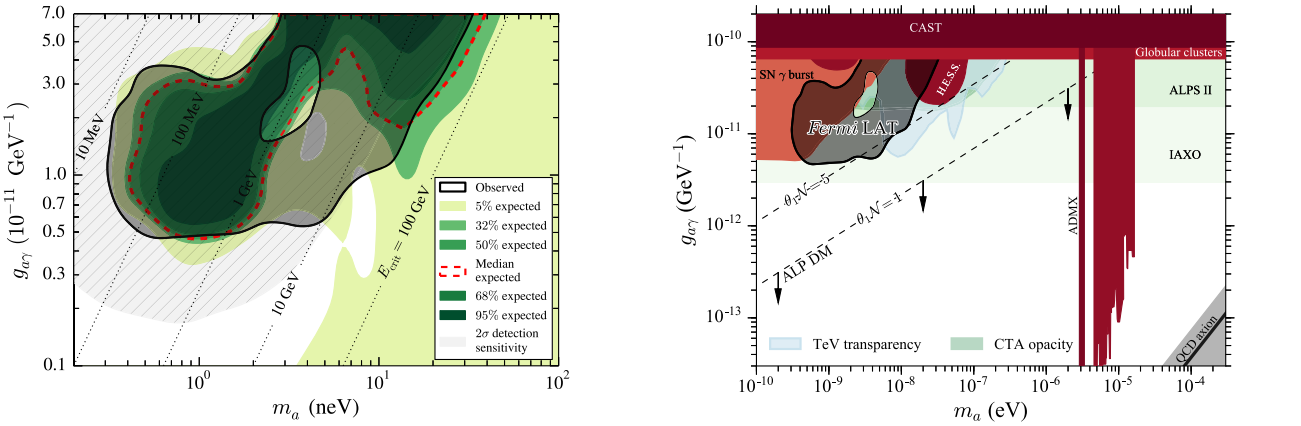

FIG. 2. Left: Observed and expected 95% confidence limits on the ALP parameters from 400 Monte Carlo simulations. Dotted lines correspond to constant critical energies. The hatched gray region shows the parameters where ALPs are detectable at the 2σ confidence level (median sensitivity). Right: Comparison of Fermi-LAT limits with other works. Other limits are shown in red, expected sensitivities in green. The parameter space where ALPs could explain a low γ-ray opacity is shown in blue. ALPs below the $\mathcal{N}\theta_1 = 1$ line could account for all the DM. The QCD axion is shown as a gray shaded band and solid black line. See, e.g., Ref. [70] and references therein.

results in overcoverage for ALP parameters causing the strongest irregularities, thus yielding conservative limits.

The excluded parameter space is shown in the left-hand panel of Fig. 2 (black shaded region). Photon-ALP couplings are ruled out between $0.5 \lesssim g_{11} \lesssim 3$ for $0.5 \lesssim m_{a,\mathrm{neV}} \lesssim 5$ and $g_{11} \gtrsim 1$ for $5 \lesssim m_{a,\mathrm{neV}} \lesssim 10$. At high masses, the limits run almost parallel to the lines of constant E_{crit} (shown as dotted lines for $B_{\mu\mathrm{G}} = 10$). For lower masses, ALP couplings along the $E_{\mathrm{crit}} = 1$ GeV line with $1.3 \lesssim g_{11} \lesssim 4$ are not excluded. Around this "holelike" feature, $P_{\gamma\gamma}$ exhibits rapid fluctuations for almost the entire Fermi-LAT energy range. Given the Poisson noise in the data, these ALP parameters cannot be excluded. We stress that the fit with ALPs is not preferred over the null hypothesis. For masses below $m_{a,\mathrm{neV}} = 0.5$, irregularities still enter the Fermi-LAT energy range, allowing us to exclude ALP parameters.

The observed limits agree well with the expected exclusion region derived from Monte Carlo simulations (shaded regions). The "hole" feature is not visible in the expected limits but occurs in certain Monte Carlo realizations (an example is given in the Supplemental Material [37]). In 5% of the simulations (yellow shaded region), ALP parameters are excluded for which the $E_{\mathrm{crit}} > 100$ GeV. This is expected since we have derived λ_{thr} from the null distribution where for 5% of the simulations one finds $\mathrm{TS} > \lambda_{\mathrm{thr}}$. The parameters for which we could detect an ALP signal at a 2σ level agree well with the observed limits (gray hatched region; see the Supplemental Material for details [37]).

The results are subject to systematic uncertainties related to the analysis and magnetic-field parameters. Concerning the analysis, changing the energy dispersion has the strongest effect on the limits. If we conservatively broaden the energy dispersion by 20%, the area of the tested ALP parameter grid with $\lambda > 22.8$ decreases by 25%. All other tested effects related to the analysis change the limits at most by ~4%. Concerning the choice of B-field parameters, neither the strength, the power spectrum, nor the dependence on the electron density of the magnetic field are well established for Perseus. Therefore, the full analysis is repeated for a magnetic-field strength of $\sigma_B = 20\mu$G, for a Kolmogorov-type turbulence spectrum, $q = -11/3$ (as found in the cool-core cluster Hydra A [62]), and by conservatively assuming that the magnetic field is zero beyond $r_{\mathrm{max}} = 100$ kpc. Increasing σ_B increases the excluded area by 43%. In comparison, the other tested parameters have a subdominant effect of maximally 16%. The dependence of the limits on the particular choice of the EBL model is negligible due to the relative proximity of NGC 1275 ($z = 0.017559$). The absorption is maximally ~8% at 500 GeV with significantly smaller relative differences for a number of EBL models [54,71–75]. We provide a comprehensive summary of all tested systematic uncertainties in the Supplemental Material [37].

The limits derived in this work are compared to other limits and sensitivities of future experiments in Fig. 2 (right). Our results give the strongest constraints to date for $0.5 \lesssim m_{a,\mathrm{neV}} \lesssim 20$ and surpass the expected limits for the planned ALPS II experiment [76] in that range. They are only a factor of ~2 below the exclusion prospects of the planned IAXO experiment [77]. We note that the systematic uncertainties of the future experiments are likely to be smaller than the ones that apply to the present analysis. In conjunction with other limits taken at face value [29,56,69], the parameter space where ALPs could explain hints for a lower γ-ray opacity compared to EBL-model predictions (light blue region) [25] is now

strongly constrained. The limits do not constrain ALPs that could make up the entire DM content of the Universe. This corresponds to the region in Fig. 2 (right) below the $\theta_1\mathcal{N} = 1$ line, where $\mathcal{N}$ is a model-dependent factor and θ_1 is the misalignment angle [10]. Our analysis only constrains ALPs that make up less than 4% of the DM, or equivalently $\theta_1\mathcal{N} > 5$.

Observations with future γ-ray instruments could improve the reported limits and test ALP DM models. The planned Gamma-400 satellite, with an envisaged energy resolution of 1% above 10 GeV [78], might be able to better resolve the spectra and probe higher ALP masses. Higher masses could also be reached with the future Cherenkov Telescope Array (CTA) [79].

It will be possible to reduce the uncertainties of the intracluster B field with the upcoming Square Kilometer Array (SKA) that will conduct a full-sky polarization survey [80]. It is expected that SKA will observe hundreds of RMs of background sources for the most massive clusters, thereby enabling a more precise determination of their magnetic fields [81].

The analysis presented here can be easily extended to other sources that reside in clusters (e.g., M 87 in the Virgo cluster) or in general to any source where ALP-induced spectral irregularities are expected. ALP parameters not constrained in the present analysis (such as those of the holelike feature) could be probed with the different B-field configurations in other sources.

The Fermi-LAT Collaboration acknowledges support for LAT development, operation, and data analysis from NASA and DOE (U.S.), CEA/Irfu and IN2P3/CNRS (France), ASI and INFN (Italy), MEXT, KEK, and JAXA (Japan), and the K. A. Wallenberg Foundation, the Swedish Research Council, and the National Space Board (Sweden). Science analysis support in the operations phase from INAF (Italy) and CNES (France) is also gratefully acknowledged. J. C. is a Wallenberg Academy Fellow. S. G. and N. M. are NASA Postdoctoral Program Fellows. M. R. is funded by Contract No. FIRB-2012-RBFR12PM1F from the Italian Ministry of Education, University and Research (MIUR).

*conrad@fysik.su.se
†manuel.meyer@fysik.su.se
‡sanchezconde@fysik.su.se
§Permanent address: Naval Research Laboratory, Washington, DC 20375, USA.

[1] J. Jaeckel and A. Ringwald, Annu. Rev. Nucl. Part. Sci. **60**, 405 (2010).
[2] R. D. Peccei and H. R. Quinn, Phys. Rev. Lett. **38**, 1440 (1977).
[3] S. Weinberg, Phys. Rev. Lett. **40**, 223 (1978).
[4] F. Wilczek, Phys. Rev. Lett. **40**, 279 (1978).
[5] E. Witten, Phys. Lett. B **149**, 351 (1984).
[6] A. Ringwald, J. Phys. Conf. Ser. **485**, 012013 (2014).
[7] J. Preskill, M. B. Wise, and F. Wilczek, Phys. Lett. B **120**, 127 (1983).
[8] L. F. Abbott and P. Sikivie, Phys. Lett. B **120**, 133 (1983).
[9] D. J. E. Marsh, Phys. Rev. D **83**, 123526 (2011).
[10] P. Arias, D. Cadamuro, M. Goodsell, J. Jaeckel, J. Redondo, and A. Ringwald, J. Cosmol. Astropart. Phys. 6 (2012) 013.
[11] G. Raffelt and L. Stodolsky, Phys. Rev. D **37**, 1237 (1988).
[12] P. Sikivie, Phys. Rev. Lett. **51**, 1415 (1983).
[13] K. A. Hochmuth and G. Sigl, Phys. Rev. D **76**, 123011 (2007).
[14] A. de Angelis, O. Mansutti, and M. Roncadelli, Phys. Lett. B **659**, 847 (2008).
[15] D. Hooper and P. D. Serpico, Phys. Rev. Lett. **99**, 231102 (2007).
[16] D. Wouters and P. Brun, Phys. Rev. D **86**, 043005 (2012).
[17] A. De Angelis, M. Roncadelli, and O. Mansutti, Phys. Rev. D **76**, 121301 (2007).
[18] M. Simet, D. Hooper, and P. D. Serpico, Phys. Rev. D **77**, 063001 (2008).
[19] A. De Angelis, O. Mansutti, M. Persic, and M. Roncadelli, Mon. Not. R. Astron. Soc. **394**, L21 (2009).
[20] A. De Angelis, G. Galanti, and M. Roncadelli, Phys. Rev. D **84**, 105030 (2011).
[21] D. Horns and M. Meyer, J. Cosmol. Astropart. Phys. 2 (2012) 033.
[22] G. Rubtsov and S. Troitsky, JETP Lett. **100**, 355 (2014).
[23] M. A. Sánchez-Conde, D. Paneque, E. Bloom, F. Prada, and A. Dominguez, Phys. Rev. D **79**, 123511 (2009).
[24] A. Domínguez, M. A. Sánchez-Conde, and F. Prada, J. Cosmol. Astropart. Phys. 11 (2011) 020.
[25] M. Meyer, D. Horns, and M. Raue, Phys. Rev. D **87**, 035027 (2013).
[26] G. Galanti, M. Roncadelli, A. De Angelis, and G. F. Bignami, arXiv:1503.04436.
[27] J. Biteau and D. A. Williams, Astrophys. J. **812**, 60 (2015).
[28] A. Domínguez and M. Ajello, Astrophys. J. **813**, L34 (2015).
[29] A. Abramowski *et al.* (H.E.S.S. Collaboration), Phys. Rev. D **88**, 102003 (2013).
[30] M. Ackermann *et al.* (Fermi-LAT Collaboration), Astrophys. J. **810**, 14 (2015).
[31] J. Aleksić *et al.* (MAGIC Collaboration), Astron. Astrophys. **564**, 13 (2014).
[32] F. Tavecchio and G. Ghisellini, Mon. Not. R. Astron. Soc. **443**, 1224 (2014).
[33] G. B. Taylor, N. E. Gugliucci, A. C. Fabian , J. S. Sanders, G. Gentile, and S. W. Allen, Mon. Not. R. Astron. Soc. **368**, 1500 (2006).
[34] W. Atwood, A. Albert, L. Baldini *et al.*, arXiv:1303.3514.
[35] M. Ackermann *et al.* (Fermi-LAT Collaboration), Astrophys. J. Suppl. Ser. **222**, 5 (2016).
[36] See http://www.slac.stanford.edu/exp/glast/groups/canda/lat_Performance.htm.
[37] See Supplemental Material at http://link.aps.org/supplemental/10.1103/PhysRevLett.116.161101, which includes Refs. [36–46], for details on the energy dispersion matrices, the used formalism to calculate photon-axionlike-particle oscillations, and details on the statistical method. We also give a comprehensive list of all tested systematic uncertainties.

[38] M. Ackermann *et al.* (Fermi-LAT Collaboration), Astrophys. J. Suppl. Ser. **203**, 4 (2012).
[39] A. Mirizzi and D. Montanino, J. Cosmol. Astropart. Phys. 12 (2009) 004.
[40] A. Mirizzi, G. G. Raffelt, and P. D. Serpico, Phys. Rev. D **76**, 023001 (2007).
[41] A. Dobrynina, A. Kartavtsev, and G. Raffelt, Phys. Rev. D **91**, 083003 (2015).
[42] D. Horns, L. Maccione, M. Meyer, A. Mirizzi, D. Montanino, and M. Roncadelli, Phys. Rev. D **86**, 075024 (2012).
[43] N. Bassan, A. Mirizzi, and M. Roncadelli, J. Cosmol. Astropart. Phys. 05 (2010) 010.
[44] S. S. Wilks, Ann. Math. Stat. **9**, 60 (1938).
[45] G. Cowan, K. Cranmer, E. Gross, and O. Vitells, Eur. Phys. J. C **71**, 1554 (2011).
[46] M. Ackermann *et al.* (Fermi-LAT Collaboration), Phys. Rev. D **91**, 122002 (2015).
[47] A. Albert, G. A. Gómez-Vargas, M. Grefe, C. Muñoz, C. Weniger, E. D. Bloom, E. Charles, M. N. Mazziotta, and A. Morselli, J. Cosmol. Astropart. Phys. 10 (2014) 023.
[48] A. Bonafede, L. Feretti, M. Murgia, F. Govoni, G. Giovannini, D. Dallacasa, K. Dolag, and G. B. Taylor, Astron. Astrophys. **513**, A30 (2010).
[49] Y. Grossman, S. Roy, and J. Zupan, Phys. Lett. B **543**, 23 (2002).
[50] A. Mirizzi, G. G. Raffelt, and P. D. Serpico, in *Axions*, Lecture Notes in Physics Vol. 741, M. Kuster, G. Raffelt, and B. Beltrán (Berlin Springer Verlag, Heidelberg, 2008), p. 115.
[51] C. Csáki, N. Kaloper, M. Peloso, and J. Terning, J. Cosmol. Astropart. Phys. 05 (2003) 005.
[52] M. Meyer, D. Montanino, and J. Conrad, J. Cosmol. Astropart. Phys. 09 (2014) 003.
[53] R. Jansson and G. R. Farrar, Astrophys. J. **757**, 14 (2012).
[54] A. Domínguez, J. R. Primack, D. J. Rosario *et al.*, Mon. Not. R. Astron. Soc. **410**, 2556 (2011).
[55] A. Ayala, I. Domínguez, M. Giannotti, A, Mirizzi, and O. Straniero, Phys. Rev. Lett. **113**, 191302 (2014).
[56] A. Payez, C. Evoli, T. Fischer, M. Giannotti, A. Mirizzi, and A. Ringwald, J. Cosmol. Astropart. Phys. 02 (2015) 006.
[57] K. Dolag, A. M. Bykov, and A. Diaferio, Space Sci. Rev. **134**, 311 (2008).
[58] Y. Dubois and R. Teyssier, Astron. Astrophys. **482**, L13 (2008).
[59] L. Feretti, G. Giovannini, F. Govoni, and M. Murgia, Astron. Astrophys. Rev. **20**, 54 (2012).
[60] E. Churazov, W. Forman, C. Jones, and H. Böhringer, Astrophys. J. **590**, 225 (2003).
[61] J. Aleksić *et al.* (MAGIC Collaboration), Astron. Astrophys. **541**, A99 (2012).
[62] P. Kuchar and T. A. Enßlin, Astron. Astrophys. **529**, A13 (2011).
[63] V. Vacca, M. Murgia, F. Govoni, L. Feretti, G. Giovannini, R. A. Perley, and G. B. Taylor, Astron. Astrophys. **540**, A38 (2012).
[64] M. Ackermann *et al.* (Fermi-LAT Collaboration), Phys. Rev. D **89**, 042001 (2014).
[65] M. Ackermann *et al.* (Fermi-LAT Collaboration), Phys. Rev. Lett. **115**, 231301 (2015).
[66] See http://fermi.gsfc.nasa.gov/ssc/data/analysis/.
[67] See http://fermi.gsfc.nasa.gov/ssc/data/access/lat/BackgroundModels.html.
[68] This procedure will result in different best-fit estimators for the source parameters for each event type. In this way, it is possible to speed up the optimization considerably. We have verified that our results do not change when the parameters of NGC1275 are tied over the event types.
[69] D. Wouters and P. Brun, Astrophys. J. **772**, 44 (2013).
[70] M. Meyer and J. Conrad, J. Cosmol. Astropart. Phys. 12 (2014) 016.
[71] A. Franceschini, G. Rodighiero, and M. Vaccari, Astron. Astrophys. **487**, 837 (2008).
[72] J. D. Finke, S. Razzaque, and C. D. Dermer, Astrophys. J. **712**, 238 (2010).
[73] T. M. Kneiske and H. Dole, Astron. Astrophys. **515**, A19 (2010).
[74] R. C. Gilmore, R. S. Somerville, J. R. Primack, and A. Domínguez, Mon. Not. R. Astron. Soc. **422**, 3189 (2012).
[75] Y. Inoue, S. Inoue, M. A. R. Kobayashi, R. Makiya, Y. Niino, and T. Totani, Astrophys. J. **768**, 197 (2013).
[76] R. Bähre, B. Döbrich, J. Dreyling-Eschweiler *et al.*, J. Instrum. **8**, T09001 (2013).
[77] I. G. Irastorza, F. T. Avignone, G. Cantatore *et al.*, J. Phys. Conf. Ser. **460**, 012002 (2013).
[78] P. Cumani, A. M. Galper, V. Bonvicini *et al.*, arXiv:1502.02976.
[79] M. Actis *et al.* (CTA Consortium), Exp. Astron. **32**, 193 (2011).
[80] B. M. Gaensler, R. Beck, and L. Feretti, New Astron. Rev. **48**, 1003 (2004).
[81] A. Bonafede, F. Vazza, M. Brüggen, T. Akahori, E. Carretti *et al.*, *Proc. Sci.*, AASKA14 095 (2015).